AIAA JOURNAL
Vol. 30, No. 8, August 1992

Control-Structure Integrated Design

Achille Messac*
Charles Stark Draper Laboratory, Inc., Cambridge, Massachusetts 02139
and
Kamal Malek†
Massachusetts Institute of Technology, Cambridge, Massachusetts 02139

This article presents an optimization-based approach to the integrated control and structural design of dynamical systems. The framework of a general formulation is developed, which lends itself directly to the design of structural plants requiring control. This method can employ classical and modern control techniques in the time or frequency domain. A performance norm that possesses full knowledge of the control and structural design characteristics is developed. This article explicitly addresses the disturbance-rejection and command-following performance of the system, in addition to the vibration level and the control effort. The design methodology is demonstrated by simultaneously performing the structural and control designs of a truss-like spacecraft undergoing a rotational maneuver.

Introduction

FUTURE military and commercial space systems will present increasingly stringent performance requirements. In order to meet the challenge, prevailing design methods must be readdressed. Current design practices are characterized by a schism between the structural and the control design processes. These two design phases are performed *separately*, following two disparate paths, with little or no interaction. This lack of interdisciplinary activity is not surprising however. Recent advances in computer technology are only beginning to have their full impact, and the development of effective control-structure integrated design (CSID) methods is far from being a solved problem. This publication takes only a step in that direction.

The structural engineer generally designs a structural plant by relying on: 1) an overall knowledge of the mission objectives and constraints, 2) some limited understanding of the control issues, and 3) experience and intuition. The typical structural design follows some iterative ad-hoc approach that often converges satisfactorily, or follows some form of structural optimization. Unfortunately, the typical structural optimization approach fails to recognize the properties of the as-yet-unknown control design.

The major limitation of structural optimization alone stems from the objective function's inability to reflect total system performance. Typical objectives include: 1) minimum mass, 2) uniform stress, 3) maximum fundamental frequency, and 4) maximum damping. For instance, by indiscriminately increasing damping and stiffness in order to meet stringent pointing requirements, structural optimization may result in large system mass, and a correspondingly high control authority requirement.

With a structural design in near-final form and an in-depth knowledge of mission objectives and constraints, the control engineers generally have at their disposal all the information needed to design a control system. Unfortunately, the control design phase has no appreciable impact on the structural design.

As a result of this limited interdisciplinary interaction, the final system design is seldom optimal in any global sense. This is particularly true in the case of complex systems where experience or intuition usually fails to produce optimal (or near-optimal) designs. In addition, although a control designer can easily determine the consequences of a control-design modification on performance, the same is not true of the structural designer. The latter's only recourse is experience and intuition.

A new approach to designing dynamical systems with improved performance and robustness characteristics has been under development for the past decade. References 1–9 represent but a small sample of the publications on the topic. This paper refers to this new approach as CSID. By recognizing the interrelated nature of the various system characteristics, and by explicitly representing the global mission objective, an optimal balance between the structure and the control system can be achieved. This design approach is characterized by full use of interdisciplinary knowledge throughout the design process. Significant required structural changes can be identified and effected early in the design process, when the cost consequences are less severe. Given typical mass constraints and the trend toward more stringent performance requirements, CSID methods must be exploited for the successful design of current and future space systems.[7]

The approach presented in this paper is highly computational in nature. Closed-form analytical solutions for the objective and constraints are employed in conjunction with nonlinear numerical optimization techniques. A scalar measure of system performance is minimized, subject to certain practical constraints. These constraints may include system stability, system mass, structural member sizes, and robustness. The existence of a closed-form solution for any performance measure is critical to the computational feasibility of CSID for realistically large structures.

In the current approach, CSID nonlinear constrained optimization is performed within a general framework. Modal reduction is employed to reduce computational effort. The structural design variables are chosen to effect mass, stiffness, and possibly damping redistribution. The control design variables are also general in nature. They can represent, among other things, elements of feedback matrices, Q-parameterization, or pole and zero location. LQR and LQG designs constitute a natural subset of the possible applications.

There are strong advantages to the computational approach advocated in this paper. Nonlinear programming methods

Received May 22, 1991; revision received Nov. 25, 1991; accepted for publication Nov. 27, 1991.

*Senior Member of the Technical Staff. Member AIAA.
†Doctoral Candidate, Department of Mechanical Engineering.

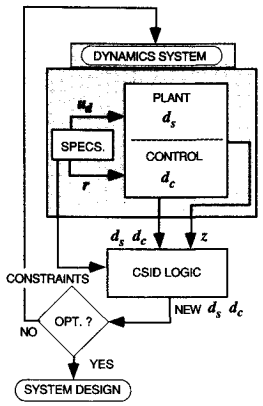

Fig. 1 CSID computational structure.

allow for explicit constraints on system characteristics. Time domain specifications (settling time due to step commands, for example) and frequency domain requirements can be formulated as constraints. A purely analytical approach would not offer such versatility.

Using this computational approach, CSID research can focus on rendering *existing* control synthesis tools applicable to CSID.

As Fig. 1 shows, a top-level view of the CSID computational structure depicts a dynamical system with performance and robustness properties that are altered by a set of control and structural design parameters. The constituent components of the CSID-logic block include numerically well-conditioned constraint and objective functions. These are nonconvex functions of the design variables. The objective function is quadratically dependent on the error vector $z(t)$. The plant-and-control design block comprises a state-space representation of the closed-loop system, which, in general, is a highly nonlinear function of the structural and control design variables d_s and d_c. The inputs to the plant/control system are the exogenous disturbance vector $u_d(t)$ and the reference signal vector $r(t)$, which have temporal or spectral properties that are dictated by system design specifications. The vector $z(t)$ denotes system response errors that the CSID-logic functional block attempts to minimize. These may include structural vibration, control effort, or pointing error.

This paper is organized as follows. First, the full-order and reduced-order modeling of the structural system is developed. Second, a general framework for compensator modeling is presented. Third, a new performance norm that addresses explicitly the command-following and disturbance-rejection properties of the system is developed. Its favorable computational properties were evidenced by successful CSID application. Fourth, the dynamics model of a truss-like spacecraft is developed, and pertinent structural parameters are identified for CSID application. Finally, the *Results and Discussion* section shows the power of CSID to identify improved system designs.The advantage of using CSID, rather than control optimization alone, is quantified.

Plant Dynamics Modeling

Physical Coordinate Representation

The plant considered in this paper consists of a structural system with governing dynamics equations that are assumed to obey the well-known set of coupled second-order differential equations. Applying finite element methods, the equations are written in the form

$$M(d_s)\ddot{q} + D(d_s)\dot{q} + K(d_s)q = B_{qc}u_c + B_{qd}u_d \qquad (1)$$

where M, D, and K respectively denote the mass, damping, and stiffness matrices that depend on a set of structural design variables d_s. These variables are capable of altering the geometrical properties of the structure and its mass, damping, and stiffness distributions. The vector q denotes the physical coordinates of the structure; u_c and u_d are the control and disturbance forces and torques, respectively, while B_{qc} and B_{qd} denote the corresponding influence coefficient matrices. The above segregation of controls and disturbances will later allow addressing the command-following and disturbance-rejection problems (Eqs. (42–43)). The specific time history of u_d is in general unknown; only some of its time or frequency domain characteristics are assumed. In this article, the vector u_d is assumed to be composed of impulses of known intensities.

For analytical convenience, we construct a standard state space representation of Eq. (1), and append observation and error equations, thus:

$$\dot{x}_q = A_q x_q + B_{xc}u_c + B_{xd}u_d \qquad (2)$$

$$z_p = C_{zq}x_q + D_q u_c \qquad (3)$$

$$y = C_{yq}x_q \qquad (4)$$

The vectors y and z_p are, respectively, the observation and error vectors. The state vector is

$$x_q = \begin{bmatrix} q \\ \dot{q} \end{bmatrix} \qquad (5)$$

The plant error vector does not include u_d because u_d cannot be minimized. The dynamics matrix takes the form

$$A_q(d_s) = \begin{bmatrix} 0 & I \\ -M^{-1}K & -M^{-1}D \end{bmatrix} \qquad (6)$$

The influence coefficient matrices are

$$B_{xc} = \begin{bmatrix} 0 \\ M^{-1}B_{qc} \end{bmatrix}, \qquad B_{xd} = \begin{bmatrix} 0 \\ M^{-1}B_{qd} \end{bmatrix} \qquad (7)$$

Equations (2–7) govern the plant dynamics. These equations are generally adequate for the analysis of low-order structural systems. In the case of large structures, however, model order reduction is required.

Modal Coordinate Representation

With high-order structural applications in mind, plant model reduction is performed via model decomposition. A linear transformation is performed, based on a subset of the modal space basis. The transformation is

$$q = \Phi\eta \qquad (8)$$

Normalization and other required definitions take the form

$$\Phi^T M\Phi = I, \qquad \Phi^T D\Phi = D_\eta, \qquad \Phi^T K\Phi = \Lambda \qquad (9)$$

$$\Lambda_{ij} = \lambda_i \delta_{ij} \qquad (10)$$

where δ_{ij} is the Dirac delta function, and

$$D_\eta \equiv D_\eta(d_s), \qquad \Lambda \equiv \Lambda(d_s), \qquad \Phi \equiv \Phi(d_s) \qquad (11)$$

The quantities Φ and Λ respectively denote the truncated modal and eigenvalue matrices of the system. The matrix D_η denotes modal damping, and takes a diagonal form in the case of low viscous damping.

The reduced-order form of the state equation is again written in its generic form as

$$\dot{x}_\eta = A_\eta x_\eta + B_{\eta c}u_c + B_{\eta d}u_d \qquad (12)$$

$$z_p = C_{z\eta}x_\eta + D_\eta u_c \tag{13}$$

$$y = C_{y\eta}x_\eta \tag{14}$$

where the modal state vector is

$$x_\eta = \begin{bmatrix} \eta \\ \dot{\eta} \end{bmatrix} \tag{15}$$

The state equation dynamical matrix reads

$$A_\eta(d_s) = \begin{bmatrix} 0 & I \\ -\Lambda & -D_\eta \end{bmatrix} \tag{16}$$

The influence coefficient matrices are

$$B_{\eta c}(d_s) = \begin{bmatrix} 0 \\ \Phi^T B_{qc} \end{bmatrix}, \quad B_{\eta d}(d_s) = \begin{bmatrix} 0 \\ \Phi^T B_{qd} \end{bmatrix} \tag{17}$$

The output and error coefficient matrices are

$$C_{y\eta} = C_{yq}\Phi \tag{18}$$

$$C_{z\eta} = C_{zq}\Phi, \quad D_\eta = D_q \tag{19}$$

Compensator Representation

The compensator employed in this paper assumes the generic form of a matrix transfer function. Specifically, for a multiple-input-multiple-output (MIMO) system, the compensator dynamics take the form

$$u_c(s) = G_c(s)^{(k\times l)} z_c(s) \tag{20}$$

where u_c and z_c respectively denote the generalized control and the error vectors, and $G_c(s)$ denotes the compensator transfer function matrix. The constituent elements of $G_c(s)$ are expressed as

$$[G_s(s)]_{ij} = \frac{\left[g \prod_{k=1}^{n1} (s + a_k) \prod_{k=1}^{n2} (s^2 + b_k s + c_k) \right]_{ij}}{\prod_{k=1}^{n3} (s + d_k) \prod_{k=1}^{n4} (s^2 + e_k s + f_k)} \tag{21}$$

where the quantities g, a_k, b_k, . . . , f_k are parameters that characterize the properties of the controller, and the indices i and j denote the (ij)th element of the transfer matrix $G_c(s)$. These parameters collectively constitute the set of control design variables.

By defining

$$v_{ij} = \{g, a_1, \ldots, a_{n1}, b_1, \ldots, b_{n2}, c_1, \ldots, c_{n2}\}_{ij} \tag{22}$$

and

$$w = \{d_1, \ldots, d_{n3}, e_1, \ldots, e_{n4}, f_1, \ldots, f_{n4}\} \tag{23}$$

the control design variable vector becomes

$$\boldsymbol{d}_c = \{v_{11}, \ldots, v_{1l}, \ldots, v_{k1}, \ldots, v_{kl}, w\} \tag{24}$$

As can be seen, the number of design variables can grow rapidly for MIMO systems. Fortunately, in practice the matrix compensator transfer function is not necessarily fully populated, nor comprised of elements of high order.

Initial values for the control variables can be obtained through conventional means such as using Matlab with the initial model of the plant. Because the CSID method in this paper is performed in state space, the state equation representation of the compensator is obtained in the standard form

$$\dot{x}_c(t) = A_c x_c(t) + B_c z_c(t) \tag{25}$$

$$u_c(t) = C_c x_c(t) + D_c z_c(t) \tag{26}$$

where x_c denotes the controller state vector and the matrices take on standard definitions. With the development of both plant and compensator, it is possible to form the closed-loop representation of the system.

Closed-Loop Representation

The state equations of the closed-loop system are obtained by combining the structure (Eqs. (12–14)) and the controller (Eqs. (25) and (26)), and by defining the error variable as

$$z_c(t) = r(t) - y(t) \tag{27}$$

It is recognized that the inputs to the global system are $r(t)$, the command reference signal, and $u_d(t)$, the disturbance. As Fig. 2 shows, the outputs are $z(t)$ and $y(t)$. The closed-loop representation is readily obtained as

$$\dot{x}_t(t) = A_t x_t(t) + B_{td}u_d(t) + B_{tr}r(t) \tag{28}$$

$$z = C_{tz}x_t + D_{tr}r \tag{29}$$

$$y = C_{ty}x_t \tag{30}$$

where

$$x_t = \begin{Bmatrix} x_\eta \\ x_c \end{Bmatrix}, \quad z = \begin{Bmatrix} z_p \\ z_c \end{Bmatrix} \tag{31}$$

$$A_t = \begin{bmatrix} A_\eta - B_{\eta c}D_c C_{\eta y} & B_{\eta c}C_c \\ -B_c C_{\eta y} & A_c \end{bmatrix} \tag{32}$$

$$B_{td} = \begin{bmatrix} B_{\eta d} \\ 0 \end{bmatrix}, \quad B_{tr} = \begin{bmatrix} B_{\eta c}D_c \\ B_c \end{bmatrix} \tag{33}$$

$$C_{tz} = \begin{bmatrix} C_{\eta z} - D_\eta D_c C_{\eta y} & D_\eta C_c \\ -C_{\eta y} & 0 \end{bmatrix} \tag{34}$$

$$D_{tr} = \begin{bmatrix} D_\eta D_c \\ I \end{bmatrix}, \quad C_{ty} = [C_{\eta y}\ 0] \tag{35}$$

Performance Norm

In this section, a norm is developed that quantifies the system performance with regard to both command-following and disturbance-rejection properties. The norm will be expressed as the infinite-time quadratic integral of the error vector $z(t)$. As is shown in Fig. 2, the system state response is due to the disturbance input $u_d(t)$, and to the reference input $r(t)$. The disturbance is assumed to take the form of a set of impulses, while the reference input is represented by a

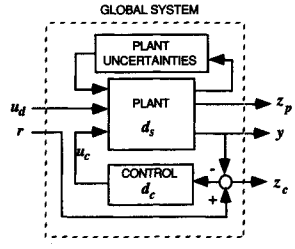

Fig. 2 Closed-loop system.

prescribed set of step commands. Therefore, the system state vector time history is expressed as

$$x_t(t) = e^{A_t(t-\tau)}x_t(\tau) + \int_\tau^t e^{A_t(t-\sigma)} [B_{td}u_d(\sigma) + B_{tr}r(\sigma)]\mathrm{d}\sigma \quad (36)$$

To obtain an expression for $z(t)$ when τ and $x_t(0)$ are set to zero, one first writes the sum of the separate contributions of reference and disturbance input as

$$z(t) = z_d(t) + z_r(t) \quad (37)$$

in which case

$$x_d(t) = \int_0^t e^{A_t(t-\sigma)}B_{td}u_d(\sigma)\mathrm{d}\sigma \quad (38)$$

$$x_r(t) = \int_0^t e^{A_t(t-\sigma)}B_{tr}r(\sigma)\mathrm{d}\sigma \quad (39)$$

Specifically, let

$$r(t) = \begin{cases} 0 & ; \quad t < 0 \\ \bar{r} & ; \quad t > 0 \end{cases} \quad (40)$$

which leads to

$$z_r(t) = [D_{tr} - C_{tz}A_t^{-1}B_{tr}]\bar{r} + C_{tz}e^{A_t t}A_t^{-1}B_{tr}\bar{r} \quad (41)$$

With the appropriate framework for the controller (sufficient number of zeros, etc.), the steady-state error can be made to vanish identically, leading to

$$z_r(t) = C_{tz}e^{A_t t}A_t^{-1}B_{tr}\bar{r}\ , \ t > 0 \quad (42)$$

Similarly

$$z_d(t) = C_{tz}e^{A_t t}B_{td}\bar{u}_d\ , \ t > 0 \quad (43)$$

where $\bar{u}_d$ denotes the impulse intensity vector. The performance norm is now expressed as the infinite-time quadratic integral of the error vector $z(t)$ as (See Eq. (37))

$$J(d_s, d_c) = \frac{1}{2}\int_0^\infty (z_r + z_d)^T Q(z_r + z_d)\mathrm{d}t \quad (44)$$

or, in expanded form

$$J(d_s, d_c) = J_{rr} + 2J_{rd} + J_{dd} \quad (45)$$

where

$$J_{rr} = \frac{1}{2}\int_0^\infty z_r^T(t)Qz_r(t)\mathrm{d}t \quad (46)$$

$$J_{rd} = \frac{1}{2}\int_0^\infty z_r^T(t)Qz_d(t)\mathrm{d}t \quad (47)$$

$$J_{dd} = \frac{1}{2}\int_0^\infty z_d^T(t)Qz_d(t)\mathrm{d}t \quad (48)$$

and where the matrix Q is a symmetric positive semidefinite weighting matrix. To evaluate the above integrals, it is convenient to first perform the modal decomposition

$$A_t = X\Lambda Y,\ XY = I,\ \Lambda_{ij} \equiv \lambda_i\delta_{ij} \quad (49)$$

which leads to the new expressions

$$z_r(t) = \bar{C}e^{\Lambda t}\Lambda^{-1}\bar{B}_r\bar{r}, \qquad t > 0 \quad (50)$$

$$z_d(t) = \bar{C}e^{\Lambda t}\bar{B}_d\bar{u}_d, \qquad t > 0 \quad (51)$$

where

$$\bar{C} = C_{tz}X, \qquad \bar{B}_r = YB_{tr}, \qquad \bar{B}_d = YB_{td} \quad (52)$$

After some manipulation, one obtains

$$J_{rr}(d_s, d_c) = \tfrac{1}{2}\bar{r}^T\bar{B}_r^T S_{rr}\bar{B}_r\bar{r} \quad (53)$$

$$J_{rd}(d_s, d_c) = \tfrac{1}{2}\bar{r}^T\bar{B}_r^T S_{rd}\bar{B}_d\bar{u}_d \quad (54)$$

$$J_{dd}(d_s, d_c) = \tfrac{1}{2}\bar{u}_d^T\bar{B}_d^T S_{dd}\bar{B}_d\bar{u}_d \quad (55)$$

where

$$(S_{rr})_{ij} = -\frac{(\bar{Q})_{ij}}{\lambda_i(\lambda_i + \lambda_j)\lambda_j} \quad (56)$$

$$(S_{rd})_{ij} = -\frac{(\bar{Q})_{ij}}{\lambda_i(\lambda_i + \lambda_j)} \quad (57)$$

$$(S_{dd})_{ij} = -\frac{(\bar{Q})_{ij}}{(\lambda_i + \lambda_j)} \quad (58)$$

$$\bar{Q} = \bar{C}^T Q\bar{C} \quad (59)$$

The above performance norm offers an important tool in designing, analyzing, and evaluating high-performance systems. It is possible to trade between the disturbance-rejection and the command-following properties of the system by appropriately selecting the vectors $\bar{r}$ and $\bar{u}$. In addition, the relative intensities of structural vibrations and generalized control forces are regulated directly by appropriately structuring the plant error (Eqs. (2–4)) and the matrix Q, Eq. (44). To see this, simply write Eq. (3) in the form

$$z_p = \begin{Bmatrix} z_{pu} \\ z_{pz} \end{Bmatrix} = \begin{bmatrix} 0 \\ \bar{C}_{zq} \end{bmatrix} x_q + \begin{bmatrix} I \\ 0 \end{bmatrix} u_c \quad (60)$$

where $z_{pu}(t)$ denotes the control, and $z_{pz}(t)$ denotes the vibration level. Therefore, the plant error vector can segregate control from vibration. Moreover, it is helpful to write the error vector as (see Eqs. (31 and 60))

$$z = \begin{Bmatrix} z_p \\ z_c \end{Bmatrix} = \begin{Bmatrix} z_{pu} \\ z_{pz} \\ \cdots \\ z_c \end{Bmatrix} \quad (61)$$

and the weighting matrix, in block diagonal form, as (see Eqs. (44 and 37)). Reference 9 treat the situation where closed-loop zero eigenvalues exist.

$$Q = \left[\begin{array}{ccc:ccc} Q_{pu} & & 0 & & & \\ & & & & 0 & \\ 0 & & Q_{pz} & & & \\ \cdots & \cdots & \cdots & \cdots & \cdots & \cdots \\ & 0 & & & Q_c & \end{array}\right] \quad (62)$$

Mathematical Problem Statement

The system dynamics equations and the performance norm are now used to formulate the CSID nonlinear programming

problem formally as

$$\min_{d_s,\, d_c} \quad J(d_s, d_c) \tag{63}$$

subject to

$$\alpha_i \leq g_i(d_s, d_c) \leq \beta_i \tag{64}$$

Equation (64) denotes constraint conditions that directly control system design specifications. These constraints include: 1) nominal or robust stability, 2) system mass, 3) structural member sizes, 4) geometry, and 5) frequency and/or time domain behavior.

It is recalled that the performance measure is a highly nonlinear integral function of the system dynamics equations and, in general, is not a convex function of the control and structural design variables. The numerical conditioning properties of both the objective and constraint functions are the key to a successful solution, especially in the case of high-order structures. The performance norm developed in this paper does display highly favorable numerical conditioning properties, and its evaluation involves numerical procedures for which robust digital algorithms exist.

The commercial code GRG2 (Generalized Reduced Gradient 2)[11] was employed as the optimization module of the CSID simulation. It was found to be numerically robust. The required gradients were evaluated via finite-difference methods. As with all nonconvex optimization problems, the algorithm might converge to a local minimum. The typical safeguards are therefore in order. These include: 1) restarting the problem with a different initial condition, 2) rescaling the problem periodically during optimization, and 3) starting from a reasonable initial condition, and so forth. Unfortunately, even with those precautions, convergence to the global minimum is not guaranteed. Detailed knowledge of the nonlinear optimization method, together with deep understanding of the problem, are the real saviors.

Spacecraft Example

Problem Statement

A spacecraft is used as an example to demonstrate the CSID approach proposed in this paper (Fig. 3a). This structure consists of a central rigid hub to which two appendages are symmetrically attached. Each truss-like appendage carries a lumped mass at its tip. Under normal operation, this spacecraft undergoes planar rotational maneuvers about the inertially fixed axis $\hat{k}$. The penalty on the control effort, the tip vibration, and the command-following error are (see Eq. (62))

$$\{Q_{pu}, Q_{pz}, Q_c\} = \{0, \zeta, 1\} \tag{65}$$

It is noted that a nonzero value of the control penalty and a more complex compensator structure are effective means of further improving system response (shorter settling-time, etc.).

The geometrical symmetry, in addition to the purely rotational motion of the spacecraft, permits the assumption of an antisymmetric deformation field. Figure 3b depicts the spacecraft kinematics. The body frame is embedded at the center of the rigid hub and is denoted by the dextral triad $\hat{i}$, $\hat{j}$, $\hat{k}$. The vector u_i denotes the translational deformation of node i, and l_i denotes its longitudinal coordinate. The vector r represents the hub radius, and l represents the appendage length. The equations of motion are obtained by applying the finite element method (FEM) in conjunction with the Newton-Euler equations.

The two trusses are modeled as a set of interconnected beam elements, each representing a bay. The generic spacecraft described is assumed to comprise 50 bays (25 per appendage). All beam elements have the same length l_e, and

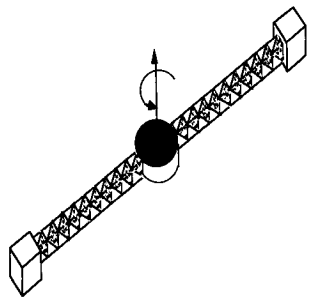

Fig. 3a Example spacecraft.

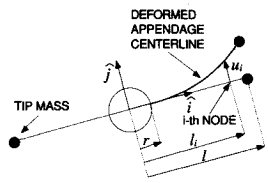

Fig. 3b Spacecraft kinematics.

the same width w. The lateral dimension of each element varies as the structure is optimized. The spacecraft inertial characteristics are modeled using a lumped mass formulation, where the nodal masses are assumed to be purely translational.

Dynamics Equations

The equation of motion development involves four steps.

Step 1: ith Mass Translational Equation

By applying Newton's law, the equation that governs the motion of the ith nodal mass along the $\hat{j}$ axis can be written as

$$m_i(\ddot{u}_i + l_i\ddot{\theta}) = f_{int,i} + f_i \tag{66}$$

where m_i is the nodal mass, θ is the inertial rotation of the hub, $f_{int,i}$ denotes the internal elastic forces, and f_i accounts for externally applied forces at node i. To obtain an explicit expression for the internal forces, the global stiffness matrix of the cantilevered truss is formed, followed by static condensation of the rotational degrees of freedom. This results in a stiffness matrix K_{tt}, which relates the internal forces to the deformation coordinates as

$$f_{int} = -K_{tt}u \tag{67}$$

The subscript tt denotes that only the *translational* degrees-of-freedom are retained in the static condensation.

Equations (66) and (67) are cast in matrix form as

$$M_{tt}\ddot{u} + S\ddot{\theta} + K_{tt}u = f \tag{68}$$

where

$$M_{tt} = \text{diag}(m_1, \ldots, m_{n-1}) \tag{69}$$

and

$$S^T = \{m_1 l_1, \ldots, m_{n-1} l_{n-1}\} \tag{70}$$

Step 2: Spacecraft Rotational Equation

The rotational equation is obtained by satisfying rotational inertial equilibrium of the spacecraft. Doing so leads to

$$I_t\ddot{\theta} + 2S^T\ddot{u} = t_{\text{hub}} + 2\sum_{i=1}^{n-1} l_i f_i \tag{71}$$

Table 1 Spacecraft properties

Spacecraft properties	Values
Tip mass	2 kg
Hub inertia I_0	4000 kg/m^2
Appendage length	20 m
Number of elements per appendage	25
Hub radius	1.0 m
Initial beam width	0.05 m
Beam depth (constant)	0.01 m
Beam volumetric density	1000 kg/m^3
Beam modulus E	10^{11} N/m^2
Damping ratio	0.5%

where

$$I_t = I_{\text{hub}} + 2\sum_{i=1}^{n-1} m_i l_i^2 \tag{72}$$

is the system total inertia, I_{hub} is the hub rotational inertia, and t_{hub} denotes the external torque applied to the hub.

Step 3: Global Equations

The global set of equations that governs the system dynamics in physical coordinates takes the form

$$M\ddot{q} + K_q = P_q F_q \tag{73}$$

where

$$q^T = \{\theta, u_1, \ldots, u_{n-1}\} \tag{74}$$

$$M = \begin{bmatrix} \frac{1}{2}I_t & S^T \\ S & M_{tt} \end{bmatrix}, \qquad K = \begin{bmatrix} 0 & 0 \\ 0 & K_{tt} \end{bmatrix} \tag{75}$$

$$P_q = \begin{bmatrix} \frac{1}{2} & l_1 & \cdots & l_{n-1} \\ 0 & 1 & \ddots & \\ \vdots & & \ddots & \\ 0 & & & 1 \end{bmatrix}, \qquad F_q = \begin{Bmatrix} t_{\text{hub}} \\ f_1 \\ \vdots \\ f_{n-1} \end{Bmatrix} \tag{76}$$

Further, let (see Eq. (1))

$$P_q F_q = B_{qc} u_c + B_{qd} u_d \tag{77}$$

$$B_{qc} = P_q E_c \tag{78}$$

$$B_{qd} = P_q E_d \tag{79}$$

where E_c and E_d are row selection matrices.

Step 4: State Equations

The full set of state equations is obtained in accordance with the notation of the dynamics modeling section. The scalars d_i denote the set of structural design variables.

System Characteristics

Two actuation cases are considered: torque at the hub, and antisymmetric forces applied along the appendages. Only hub angular position is fed back to the controller. Tip displacement is sensed and penalized via the objective function (see Eq. (65)). A 12th-order structural model was retained, and a third-order compensator with three zeros was employed. A 15th-order system model with 50 structural design variables was deemed adequate to demonstrate the current methodology.

Table 1 shows the numerical values used.

Results and Discussion

Results obtained using the above spacecraft model demonstrate the effectiveness and flexibility of the proposed CSID approach. These results show that the previously derived norm is effective and numerically well conditioned for performing control and structural optimization. It is also shown that the CSID methodology results in much improved response compared to control optimization alone. These improvements are not easily identifiable via conventional design methods.

The proposed approach is computationally robust, as all the results presented rely on a low-order compensator (third-order) and, in some cases, the sensor and actuators are not colocated. In addition, optimized designs were obtained starting with rather poor compensators. Via numerous numerical simulations, it is observed that the lower the compensator order, the worse the performance, but also the worse the numerical conditioning of the problem as a whole.

Two sets of results are presented in Figs. 4 and 5. *The first demonstrates the advantages of CSID over control optimization only. The second shows the ability of CSID to make effective use of the available mass: the mass of the appendage is allowed to vary.* In both figures, the command input is a unit-step hub rotation θ_{ref} and no disturbance inputs are used (the disturbance input weight is set at zero). Performance is characterized by the hub angle response θ and the vibration of the tip mass u_{tip}. In all cases, the tip vibration weight ζ (Eq. (65)) used in computing the objective function is 100.

The mode of actuation used for the cases of Fig. 4 (cases Ia, Ib, and Ic) is a force pair acting antisymmetrically as a couple on the appendages, at node number 16 (13.8 m from the center of the hub). For the cases in Fig. 5 (cases IIa, IIb, and III), actuation is via torque applied at the hub center.

These results are discussed in the appendix.

Advantage of CSID over Controller Optimization Only (Fig. 4)

Figure 4 contrasts control optimization alone (left column, 4L) vs CSID (right column, 4R). In Fig. 4L, control optimization is performed by optimizing the seven parameters of the third-order controller, namely *g*, *a1*, *b1*, *c1*, *d1*, *e1*, and *f1* (see Eq. (21)). A set of controller parameters are chosen

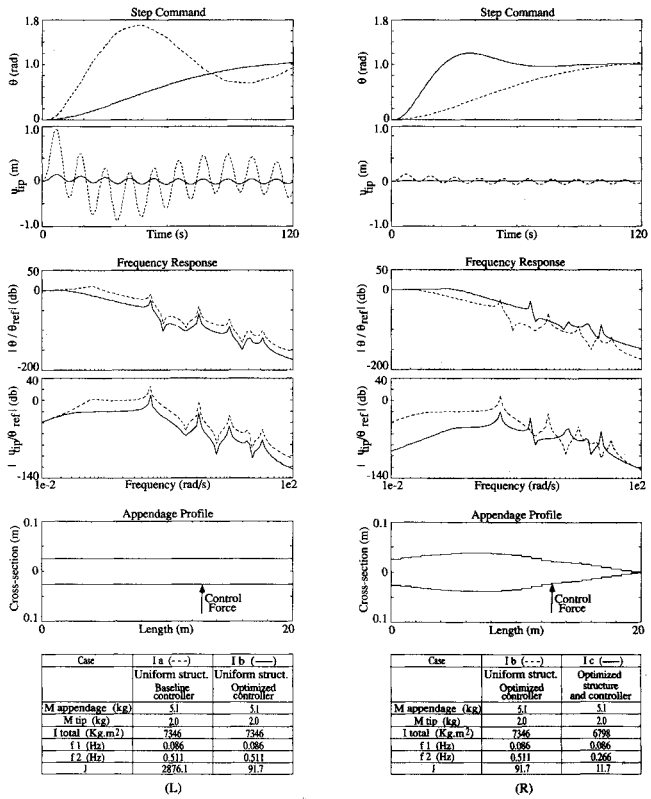

Fig. 4 Comparison between controller optimization, left column (L), and CSID, right column (R).

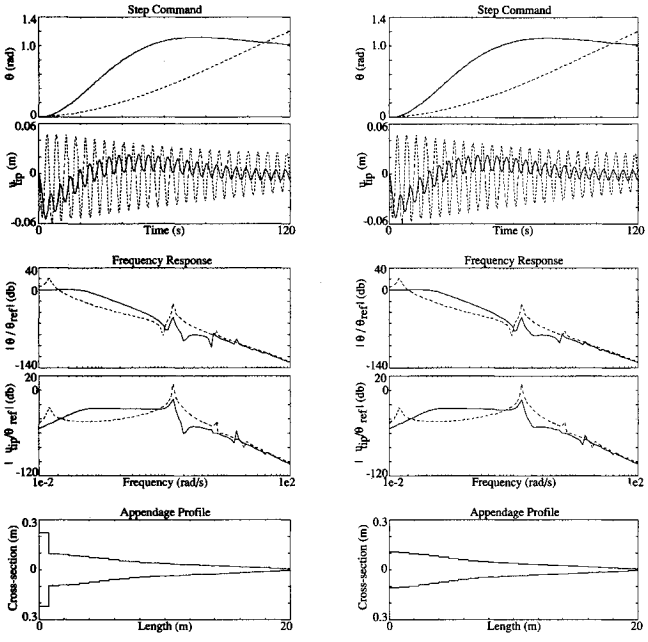

Case	IIa (- - -) Uniform struct. Baseline controller	IIb (—) CSID Constant Mass
M appendage (kg)	10.0	10.0
M tip (kg)	2.0	2.0
I total (Kg.m²)	8853	7195
f1 (Hz)	0.219	0.214
f2 (Hz)	1.063	0.937
J	392.2	24.0

(L)

Case	IIa (- - -) Uniform struct. Baseline controller	III (—) CSID Free Mass
M appendage (kg)	10.0	9.2
M tip (kg)	2.0	2.0
I total (Kg.m²)	8853	7194
f1 (Hz)	0.219	0.215
f2 (Hz)	1.063	0.930
J	392.2	23.9

(R)

Fig. 5 CSID: Comparison of constant-mass, left column (L), and free-mass, right column (R) cases.

as a starting point for the optimization. The response of the closed-loop system with that starting or baseline controller (case Ia) is shown by the dashed lines. The response of the closed-loop system using the optimized controller (see Ib) is shown by the solid lines.

The first two plots show the response to a unit step command in the reference hub angle. The starting controller results in poor response, as no significant effort was expended on its selection. The hub response exhibits an overshoot of about 80%. The tip displacement is quite large and poorly damped. The optimized controller reduces the displacement by approximately an order of magnitude. However, that improvement is achieved at the expense of the hub response, which becomes very sluggish. That performance reflects the choice of weights on control, hub position error, and tip displacement used in computing the objective function. It also reflects the low order of the controller.

The next two plots show the hub angle frequency response and the tip displacement frequency response, respectively, to a desired hub angle input. The frequency responses exhibit the same behavior already seen above. With the baseline controller, the hub response has an underdamped peak at approximately 0.7 rad/s, reflecting the overshoot in the step response. The optimized controller eliminates that peak, but also reduces the bandwidth of the system (the response visibly drops below 0 dB above 0.02 rad/s, and it stays below that of the baseline controller from that frequency on). All resonant peaks are reduced. The tip frequency response also mirrors the step response. Compared to the baseline system, the low-frequency (0.7 rad/s) peak is eliminated, which explains the absence of the low-frequency component in the step response. The amplitude of the peak at 0.5 rad/s, which corresponds to the high-frequency component of the step response, is reduced significantly: its H_∞ norm (Ref. 10) is reduced by about 20 dB. The tip response remains below that of the baseline system for all frequencies above 0.02 rad/s.

The last plot in that column shows the geometric profile of the appendages for the optimized case; that profile is uniform, as structural optimization was not allowed in this case.

The table at the bottom of the column gives some of the spacecraft parameters. The controller parameters for the various cases are given in the appendix.

Figure 4R contrasts the case of the optimized controller discussed above (case Ib), now represented by the dashed lines, to the case where structure and controller parameters are optimized concurrently using the CSID methodology (case Ic), given by the solid lines. The CSID case exhibits improved hub and tip step response. The hub response rise time is reduced from approximately 115 s to less than 35 s, with about 20% overshoot, however a consequence of the choice of weights, and of the low-order compensator used. Tip displacement response is reduced significantly.

These improvements can also be seen in the frequency response plots. Hub bandwidth is extended from about 0.02 rad/s to about 0.1 rad/s with a slightly underdamped peak. Tip response amplitude is significantly reduced (by up to 50 dB) at all frequencies up to about 1.5 rad/s.

These improvements are the result of the reshaped appendages, the profile of which is shown in the fifth plot. In terms of the objective function J (see table at bottom of each column), CSID provides a reduction by a factor of eight compared to optimizing the controller parameters only.

CSID and Mass Constraint (Fig. 5)

Figure 5 shows the ability of CSID to make effective use of the available mass. The appendage mass is first constrained to its original values (Fig. 5L), then allowed to vary (Fig. 5R). When the appendage mass is constrained, the optimization process places the excess-mass where it has the least effect (near the hub). When the appendage mass is left free, CSID removes the excess-mass, resulting in reduction of system mass. Hub torque actuation is used in this case.

The optimized CSID cases (cases IIb and III) are given by the solid lines in Figs. 5L and 5R. A baseline case (case IIa), which corresponds to a uniform nonoptimized structure, along with a third-order compensator, is given by the dashed lines for reference. Again, no serious effort was expended on tuning the baseline compensator. The only difference between the two CSID cases is the total appendage mass. In case IIb, the mass of the appendage is constrained to remain constant at 10 Kg. In case III (Fig. 5R), that constraint is removed.

It is interesting to note how the appendage mass is distributed in these two cases. Because the actuation torque is applied at the hub and no force acts on the appendage itself, the profile of the latter tapers uniformly toward the tip. In the first case (case IIb), a significant amount of mass is moved to the first element, next to the hub, in order to reduce the total rotational inertia of the system. This reflects the weights chosen for hub angle error and tip vibration (increasing the latter to 1000 causes that excess mass to get redistributed along the beam).

The hub and tip step responses do not exhibit significant differences between the two cases of interest (cases IIb and III). Similarly, the frequency responses do not differ much. The message here is: "The same level of performance could be obtained with a lighter structure." CSID was an effective avenue to finding this lighter structure. The appendage mass is reduced by about 8% in this process.

Conclusion

A new optimization-based approach to the integrated control and structural design of large space structures has been presented, and its effectiveness successfully demonstrated in the design of a maneuvering truss-like spacecraft. The computational framework of the formulation offers great versatility in that it can accommodate most state-of-the-art control techniques. A performance norm is developed, which is numerically well behaved, and particularly well suited for CSID application. Results show that the CSID approach presented in this paper provides a methodical means for obtaining both improved control and structural designs.

Table A1 Controller parameters for Fig. 5

Parameter	Case Ia: Uniform structure baseline controller $\zeta = 100$	Case Ib: Uniform structure optimized controller $\zeta = 100$	Case Ic: Optimized structure and controller (CSID) $\zeta = 100$
g	0.1500E + 1	0.1706E + 0	0.1837E + 1
a_1	0.5400E − 1	0.9541E − 6	0.9945E − 6
b_1	−0.8000E − 1	−0.3110E + 0	−0.7979E − 1
c_1	0.3900E + 1	0.3896E + 1	0.3902E + 1
d_1	0.1400E + 0	0.4162E − 1	0.1081E + 0
e_1	0.4500E + 1	0.4502E + 1	0.4499E + 1
f_1	0.2900E + 1	0.2903E + 1	0.2898E + 1

Table A2 Controller parameters for Fig. 6

Parameter	Case IIa: Uniform structure baseline controller $\zeta = 100$	Case IIb: CSID constant mass $\zeta = 100$	Case III: CSID free mass $\zeta = 100$
g	0.1500E + 2	0.1226E + 2	0.1229E + 2
a_1	0.1500E + 0	0.9579E − 6	0.9577E − 6
b_1	0.2000E + 1	−0.6129E − 1	0.5603E + 0
c_1	0.4000E + 1	0.4307E + 1	0.4308E + 1
d_1	0.1600E + 1	0.6228E − 1	0.6327E − 1
e_1	0.1000E + 1	0.4303E + 1	0.4763E + 1
f_1	0.3000E + 1	0.2784E + 1	0.2784E + 1

Appendix

The controller parameters, used in each of the cases discussed in the *Results and Discussion* section, and shown in Figs. 4 and 5, are given in the Tables A1 and A2. The parameters correspond to those defined in Eq. (21).

Acknowledgments

This work was sponsored by the Charles Stark Draper Laboratory Inc. under IR&D Project 301. The authors express their gratitude to the reviewers and to the editor for their valuable remarks and suggestions.

References

[1]Messac, A., and Turner, J. D., "Dual Structural Control Optimization of Large Space Structures," *AIAA Dynamics Specialists Conference*, Paper 84-1042-p, Palm Springs, CA, May 17–18, 1984.

[2]Messac, A., Turner, J. D., and Soosaar, K., "An Integrated Control and Minimum-Mass Structural Optimization Algorithm for Large Space Structures," NASA JPL, *Workshop on Identification and Control of Flexible Space Structures*, JPL 85-29, San Diego, CA, July 4–6, 1984.

[3]Milman, M., Salama, M., Schad, R., Bruno, R., and Gibson, J. S., *Integrated Control-Structures Design: A Multiobjective Approach*, JPL D6767, Jet Propulsion Laboratory, Pasadena, CA, Jan. 1990.

[4]Onoda, J., and Haftka, R. T., "An Approach to Structure/Control Simultaneous Optimization for Large Flexible Spacecraft," *AIAA Journal*, Vol. 25, No. 8, 1987, pp. 1133–1138.

[5]Belvin, W. K., and Park, K. C., "Structural Tailoring and Feedback Control Synthesis: An Interdisciplinary Approach," *Journal of Guidance, Control, and Dynamics*, Vol. 13, No. 3, 1990, pp. 424–429.

[6]Rao, S. S., Venkaya, V. B., and Khot, N. S., "Game Theory Approach for the Integrated Design of Structures and Controls," *AIAA Journal*, Vol. 26, No. 4, 1988, pp. 463–469.

[7]Newsom, J. R., Layman, W. E., Waites H. B., and Hayduk, R. J., "The NASA Controls-Structures Interaction Technology Program," *Forty-First Congress of the International Astronautical Federation*, Dresden, Germany, Oct. 6–12, 1990.

[8]Kirk, C. L., and Junkins, J. L., "Dynamics of Flexible Structures in Space," *Proceedings of the First International Conference at Cranfield United Kingdom*, 15–18 May 1990, Springer-Verlag, New York.

[9]Messac, A., Caswell, R., and Henderson, T., "CSID Control Structure Integrated Design: Centralized vs Decentralized Control," AIAA 1st Aerospace Design Conference, The Impact of Multidisciplinary Design Optimization, Irvine, CA, February 3–6, 1992.

[10]Maciejowski, J. M., *Multivariable Feedback Design*, Addison-Wesley, Reading, MA, 1989, p. 15.

[11]Lasdon, L. S., and Waren, E. D., *GRG2 User's Manual*, Department of General Business, School of Business Administration, Univ. of Texas, Austin, TX.